Dual Frequency Bands Shadowing Correlation Model in A Micro-cellular Environment

Daoud Burghal*, *Student Member, IEEE,* Sinh L. H. Nguyen‡,
Katsuyuki Haneda‡, *Member, IEEE,* and Andreas F. Molisch*, *Fellow, IEEE*
* University of Southern California, Los Angeles, CA USA.
‡Aalto University, School of Electrical Engineering, Finland
Email: *{burghal, molisch}@usc.edu; ‡{sinh.nguyen, katsuyuki.haneda}@aalto.fi

***Abstract*—Future wireless networks are expected to operate in both the centimeter-wave and millimeter wave bands. It is thus necessary to provide an accurate characterization of the *joint* channel properties in the two bands. Shadow fading is an important characteristic of wireless channels as it impacts achievable data rates and in particular outage probabilities. In this paper, we propose cross-band correlation models that can be used to captures the correlation over space and frequency. The models are designed to reduce to existing correlation models in the case of a single-band, which enables reuse of the large existing literature for (single-band) shadowing models. We extract and report the parameters of the proposed models in a micro-cellular environment. The important finding from our proposed models is that the cross-band spatial correlation function may not be derived just by scaling a single-band correlation function.**

I. Introduction

Shadow fading is a large scale variation of the received signal power around the distance-dependent path-loss. It is usually a result of the interaction of the transmitted signal with blocking objects and scattering surfaces in the environment [1]. The statistical characteristics of the shadowing, and in particular its correlation properties need to be considered in order to assess the impact of shadow fading on system performance and to design countermeasures [2], [3]. For this reason, the spatial correlation of shadowing has been investigated and modeled for many decades, in particular for macro-cellular communication in Sub-6 GHz frequencies for urban, suburban and rural environments [1], [4]. Recently, several new communication paradigms and models were proposed for future wireless systems; this has motivated the investigations of channel properties in new setups and environments.

Communication using different frequency bands, e.g., centimeter-wave (cmWave) and millimeter-wave (mmWave) bands, is one of the foreseen solutions for the growing demand on wireless data [5], [6]. For instance, the mmWave band can be used to provide the high data rates needed for a number of applications, but the harsh propagation conditions require the proper utilization of the more stable cmWave band, e.g., for signalling and/or as a fallback data communication band. Due to the large frequency separation, signals in the two bands interact differently with the scatterers in the same environment [1]. For instance, it was observed that in the mmWave band scattering is more pronounced, and signals are more sensitive to diffraction loss. Nevertheless, a number of recent studies indicate possible shadowing correlation over the two bands, e.g., [7].

In this paper, we provide our initial investigation of the *joint* spatial and frequency correlation properties of shadowing, and propose correlation models that consider both dimensions. The proposed models could be used, for instance, to generate shadowing realizations over the two bands, or to quantify the correlation between an observed shadowing in one band and the shadowing values in different locations in the other frequency band, for example, see [6].

As mentioned above, there has been extensive research on spatial shadowing correlation [8]. The widely used Gudmundson model, [4], assumes that the correlation value between two points decays exponentially with the separation distance. Several other extensions to this model were proposed, e.g., a double exponential and a generalized exponential-based models were proposed in [9], [10], while other models incorporate both angular and distance separation of the considered locations, for a survey see [8]. Besides the spatial correlations, other studies considered shadowing correlation across time, neighbor cells, and peer-to-peer links in multi-hop systems [8], [11], [12]. Studying the correlation across frequencies was also considered in a number of prior works [13]–[17]. Ref. [13] provides efficient methods to generate correlated shadowing realization over space and frequency domains for given correlation models. Refs. [15]–[17] reported only the correlation coefficients for the studied frequencies but did not provide models to capture the joint correlation in space and frequency. Ref. [14] suggests a frequency-only correlation model, which does *not*, in general, allow to create the joint spatial correlations between two bands. Furthermore, the majority of prior works considered closely separated frequencies in the cmWave band, which were reported to have high correlation values.

Different from the prior work, we propose shadowing correlation models across frequency bands *and* space, where we consider frequencies in the cmWave and mmWave bands. To parameterize the models, we generated channel realizations at 4 GHz and 28 GHz frequencies in a micro-cellular environment using ray-tracing with experimental validation [18]. The ray-tracer uses point cloud obtained from a high-resolution laser scan of the environment. The use of the *point cloud* for ray-based channel simulations provides good accuracy

while reducing the need for extensive concurrent measurement campaigns over the two frequency bands.

The structure of this paper is as follows. Sec. II discusses the proposed correlation models and comments on their mathematical feasibility. Sec. III, elaborates on the methodology used to generate the channel realizations and describes the considered micro-cellular environment. Sec. IV, presents the extracted path-loss and shadowing parameters. Sec. V summarizes the parameters of the models, and provides some insights about the models and the observed correlation in the considered environment. Finally, Sec. VI provides concluding remarks and highlights future work.

II. Shadowing Model

We consider a dual band wireless system that consists of a single access point (AS) located at $\boldsymbol{r}_{\mathrm{AP}}$, which can communicate over the cmWave and the mmWave bands. We use subscripts c and m to refer to the cmWave and mmWave bands respectively. The goal is to model the correlation of the shadowing values over different receivers locations in the two bands. Using the conventional power-law path-loss model [1], the received signal power in band $b \in \{c, m\}$ at location $\boldsymbol{r}_i$ is given by (on a logarithmic scale)

$$\begin{aligned} P_{\mathrm{R},b}(r_i) =& P_{\mathrm{T},b} + 10 \;.\; \epsilon_b \;.\; \log_{10}\big(D(\boldsymbol{r}_{\mathrm{AP}}, \boldsymbol{r}_i)/d_0\big) \\ &+ A_b(d_0) + S_b(\boldsymbol{r}_i). \end{aligned}$$

where $P_{\mathrm{T},b}$, $D(\boldsymbol{x}, \boldsymbol{y})$, d_0, A_b, ϵ_b, and S_b are, respectively, the transmitted power (usually a known constant), the Euclidean distance between $\boldsymbol{x}, \boldsymbol{y}$, the reference distance in meters (set to 1 m), the intercept, the path-loss exponent and the shadowing. The amplitude of the shadowing (on the logarithmic scale) is usually assumed to be normally distributed with mean zero and variance σ_b^2, i.e., $S_b \sim \mathcal{N}(0, \sigma_b^2)$. Let $C_{b,b}\big(S_b(\boldsymbol{r}_i), S_b(\boldsymbol{r}_j)\big)$ be the correlation between two receiver locations $\boldsymbol{r}_i, \boldsymbol{r}_j$ in the same band b. This single-band correlation is the classical case that has been explored for a long time, as expounded in Sec. I. A widely used model is the Gudmundson correlation model

$$C_{b,b}\big(S_b(\boldsymbol{r}_i), S_b(\boldsymbol{r}_j)\big) = \exp^{-\frac{\Delta}{d_{\mathrm{cor},b}}\ln(2)}, \tag{1}$$

where $\Delta = D(\boldsymbol{r}_i, \boldsymbol{r}_j)$, and $d_{\mathrm{cor},b}$ is usually referred to as the decorrelation distance in band b. The modified model proposed in [9] is given as below

$$C_{b,b}\big(S_b(\boldsymbol{r}_i), S_b(\boldsymbol{r}_j)\big) = \exp^{-\left(\frac{\Delta}{d_{\mathrm{cor},b}}\ln(2)\right)^{\gamma_b}}, \tag{2}$$

where $\gamma_b > 0$ is a decay exponent that impacts the curvature of the decay. In (1) and (2), $d_{\mathrm{cor},b}$ and γ_b may be environment and frequency dependent. Once the parameters, $d_{\mathrm{cor},b}$ and γ_b, are given, (1) and (2) depend on Δ only. Note that even introducing a frequency dependence of the parameters, $d_{\mathrm{cor},b}$ and γ_b, does *not* establish a model for the correlation across bands. In this paper we propose two dual-frequency correlation models that incorporate previously used single-band correlation models, i.e., our general models degenerate to the established models when only a single-band is considered. For two frequency bands b and b', it is reasonable to assume that the cross-band correlation is related to $C_{b,b}\big(S_b(\boldsymbol{r}_i), S_b(\boldsymbol{r}_j)\big)$ and $C_{b',b'}\big(S_{b'}(\boldsymbol{r}_i), S_{b'}(\boldsymbol{r}_j)\big)$. Then, our first proposed model (*model 1*) for $b \neq b'$ is:

$$\begin{aligned} C_{b,b'}\big(S_b(\boldsymbol{r}_i), S_{b'}(\boldsymbol{r}_j)\big) = \rho\Big(&\alpha_b \;.\; C_{b,b}\big(S_b(\boldsymbol{r}_i), S_b(\boldsymbol{r}_j)\big) + \\ &\alpha_{b'} \;.\; C_{b',b'}\big(S_{b'}(\boldsymbol{r}_i), S_{b'}(\boldsymbol{r}_j)\big)\Big), \end{aligned} \tag{3}$$

where $\rho \in [-1, 1]$ is the frequency correlation value which depends on the separation frequency of b, b', α_b is a "weight" for the single-band correlation in b. An intuitive relation between α_b and $\alpha_{b'}$ is $\alpha_{b'} = 1 - \alpha_b$, i.e., the cross correlation is weighted average of the two. We notice that this provides good results in the studied environment in Sec. V. For the second model (*model* 2)

$$\begin{aligned} C_{b,b'}\big(S_b(r_i), S_{b'}(r_j)\big) = \rho\Big(&C_{b,b}\big(S_b(\boldsymbol{r}_i), S_b(\boldsymbol{r}_j)\big)^{\beta_b} \times \\ &C_{b',b'}\big(S_{b'}(\boldsymbol{r}_i), S_{b'}(\boldsymbol{r}_j)\big)^{\beta_{b'}}\Big), \end{aligned} \tag{4}$$

where β_b is an exponent weight of the correlation function in band b. For (1) and (2), model 2 represents the weighted sum of the exponents. A special case is when $\beta_b = \beta_{b'} = \beta$, which will be shown to exhibit good results in Sec. V. Note that when $\beta = 0.5$ model 2 is the geometric mean of the single-band models.

A. Comment on the feasibility of the proposed model

One method to generate shadowing realizations is by first identifying the covariance matrix $\boldsymbol{\Sigma}$. For instance, to generate shadowing realizations at N locations over the two bands $\boldsymbol{\Sigma}$ is a $2N \times 2N$ matrix, the structure of $\boldsymbol{\Sigma}$ is

$$\Sigma = \begin{bmatrix} \Sigma_{b,b} & \Sigma_{b,b'} \\ \Sigma_{b',b} & \Sigma_{b',b'} \end{bmatrix}, \tag{5}$$

where $\boldsymbol{\Sigma}_{\{.,.\}}$ are $N \times N$ matrices. Note that $\boldsymbol{\Sigma}_{b,b}$, $\boldsymbol{\Sigma}_{b',b'}$, are generated using $\sigma_b^2 \times C_{b,b}$ and $\sigma_{b'}^2 \times C_{b',b'}$, respectively, while $\boldsymbol{\Sigma}_{b',b}$ and $\Sigma_{b,b'}$ are generated using $\sigma_b \sigma_{b'} \times C_{b,b'}$. $\boldsymbol{\Sigma}$ needs to be positive semi-definite (PSD) when generating Gaussian realizations. When $C_{b,b}$ and $C_{b',b'}$ are PSD, then it is easy to show that $C_{b,b'}$ is also PSD for both models [8].[1] Note that this holds for the considered single-band correlation examples: (1) is PSD in general, and (2) is PSD when $\gamma_b \in (0, 2]$. However, from (5) it is obvious that the entries of $\boldsymbol{\Sigma}$ need to be calculated from three different functions, $C_{b,b}$, $C_{b,b'}$, $C_{b',b'}$, i.e., a composite piece-wise correlation model, and the resulting models are not generally PSD [8]. In this case the generated $\boldsymbol{\Sigma}$ needs to be corrected, e.g., through methods similar to [19]. We leave further consideration of the feasibility for future work.

[1]For model 2, this true when β is integer as it represents multiplication of PSD models, which would also hold for the two single-band models (eqs. (1) and (2)).

III. Propagation channel data

In order to obtain the propagation channel data for this study, we use a point cloud-based ray-tracing channel simulations in an urban open square scenario of size 120m×120m, as shown in Fig. 1. The digital map of the environment is created via high resolution laser scanning and is in the form of a point cloud with very high accuracy and level of details. Specifically, the average sampling distance of the point cloud measurement for this environment is 10 cm, and the average range error of the laser scanner is in the order of millimeters (about 1 mm at 10 m distance, and 5 mm at 50 m distance). In order to obtain consistent channel characteristics across different frequency bands, all propagation mechanisms including specular and reduce-specular reflections, diffraction, and diffuse scattering are frequency-dependent, and calibrated with measurements in several cmWave and mmWave frequency bands [20, Section 7.4], [21, Section A.2.2]. For the diffuse scattering the Kirchhoff approximation model is used, which was shown to be effective for outdoor environments in both cmWave and mmWave frequencies [22], [23]. Specifically, thanks to the high geometric details of the map, the roughness of the local surfaces is calculated to determine the candidate points for specular and reduced-specular reflections [24]. For the diffraction, the edge points of the geometrical objects are determined, and the uniform theory of diffraction (UTD) is applied.

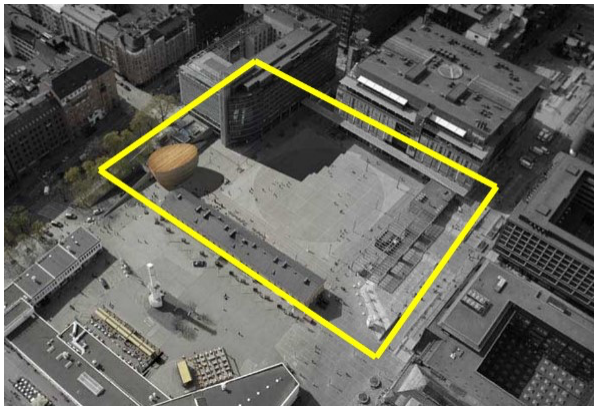

Fig. 1: Simulation scenario: open square in Helsinki.

Point cloud processing combined with visual inspection of the environment [25] is used to identify points belonging to the same object, which is assumed to have homogeneous electrical properties for specular reflections and diffuse scattering power calculations, using ITU-R P.2040 Recommendation [26]. In addition, we determine for each generated propagation path if it experiences shadowing loss or penetrates some objects in the environment, using the method in [27]. The shadowing and blockage detection method is based on the concept of first Fresnel zone clearance, which we use to determine whether a link is in a Line of Sight (LOS) condition at a specific frequency. Paths penetrating through each object are assigned a specific penetration loss value, which are calibrated with measurements at the frequencies of interest. For the sake of simplicity, only four types of material are classified and all points belonging to one type are assigned the same penetration loss value; note we use different values for different frequencies. Fig. 2 shows the point cloud of the environment where points are classified according to their assigned material. The calibrated penetration loss values are given in Table I. The remaining points that were not calibrated are classified as "rest" and their penetration loss values are obtained from a heuristic fine tuning to match the simulated channels with the measured ones at each link, then averaged over all measured links, as was previously done in [20, Section 7.4], [21, Section A.2.2], [28].

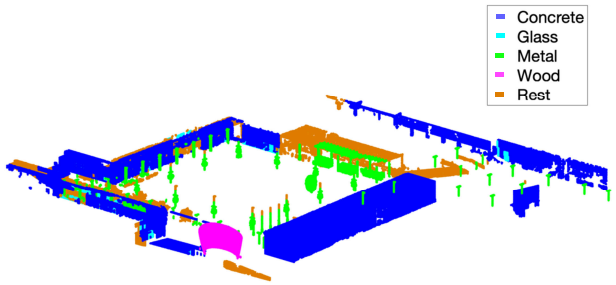

Fig. 2: Classified material point cloud.

TABLE I: Calibrated and assigned penetration losses

Object	4-GHz value	28-GHz value
Concrete wall	15 dB	50 dB
Glass window/wall	5 dB	20 dB
Lampost/Small Pillar	3 dB	8 dB
Large Pillar	5 dB	12 dB
Rest	8 dB	30 dB

TABLE II: Summary of the simulation campaign.

Parameter	4-GHz band	28-GHz band
Center frequency	4.65 GHz	27.45 GHz
Number of receiv. nodes (Rx)	3035	
Number of AP node	1	
AP / Rx height	5 / 1.5 m	
Link distance range	1 – 120 m	
Specular reflection	First- and second-order	
Diffraction	First-order	
Diffuse scattering	First-order	
Power dynamic range	40 dB	
Maximum delay	1000 ns	

In this open square, we then simulate a micro-cellular scenario where the AP is placed on a lamp-post at 5m height, and the receiver nodes are placed on a 2m×2m horizontal grid, each at 1.5m height. 3035 links, and two frequency bands (at 4 and 28 GHz) are simulated for each AP receiver link. The details of the simulation campaigns are summarized in Table II. Fig. 3 shows the simulated path gain for each band.

IV. Plath-loss and shadowing values

Here we extract the shadowing values from the generated data. In this study we focus on the Non-LOS (NLOS) scenario

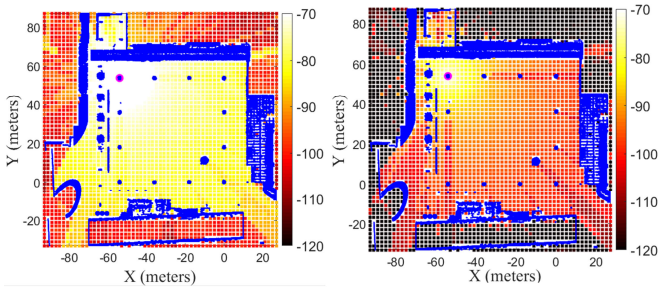

Fig. 3: Heat map of path gain at the simulated receiving positions in (a) 4 GHz and (b) 28 GHz bands.

as it typically suffers large shadowing. After a careful investigation of the data and the environment we can recognize six NLOS regions, see Fig. 4-(a). Regions 1-5 belong to points behind the interfaces of the buildings shown in Fig. 1. We do not classify the points as outdoor and indoor since for the points in regions 1-5 we have only considered the losses from the scanned interfaces, i.e., we did not consider the furniture, internal walls etc. The received powers are shown in Fig. 4-(b). Note that some points in region six belong to a cluster of partially obstructed LOS points, which shows a slope that is different from the LOS and other NLOS. Consequently, we do two linear fits for the *NLOS* points: partially obstructed LOS and fully obstructed LOS. The fitted parameters are presented in Tab. III for both frequency bands. Note that we use a single linear fit for the path-loss for the fully obstructed LOS points as it is not easy to cluster regions based on the received powers in Fig. 4-(b).

TABLE III: Basic Path Loss Shadowing Fits

Parameter	4-GHz value	28-GHz value
A_b (Obst)	-77.4 dB	-108.2 dB
ϵ_b (Obst.)	-1.23	-1.23
A_b (Part. Obst)	-56.54 dB	-81.59 dB
ϵ_b (Part. Obst)	-1.55	-1.3
σ_b	4.07 dB	9.06 dB

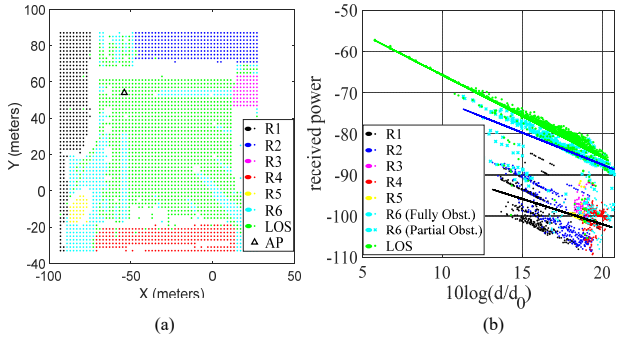

Fig. 4: (a) Distinguished regions, (b) the received power and the Path-loss fit. Three linear fits: LOS, Partially Obstructed LOS, Fully Obstructed LOS

Using the linear fits we subtract the path-loss values from the received signals to extract the NLOS shadowing values. The standard deviation of the NLOS shadowing for both frequency bands are shown in Table III. Fig. 5-(a) compares the cumulative distribution function (CDF) of the shadowing in both frequency bands to the theoretically fitted CDFs. We notice reasonable resemblance of the normal distribution. The small deviation is attributed to the small clustered regions in Fig. 4-(b); this is also observed in the 3 dimensional histogram in Fig. 5 (b).

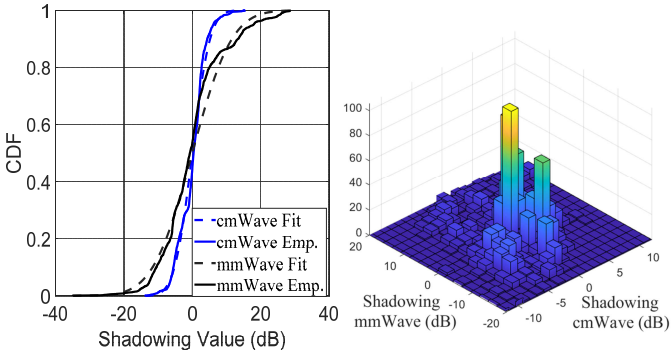

Fig. 5: (a) Empirical shadowing distribution against the fitted CDF distribution, (b) 3D histogram of the shadowing values.

V. Shadowing Correlation

In this section we analyze the empirical correlation over the two bands, and then fit it to the proposed models. To calculate the correlation, define the *sets* of locations pairs

$$\mathcal{G}_n = \big\{(\boldsymbol{r}_i, \boldsymbol{r}_j) : (n-1)\delta \le D(\boldsymbol{r}_i, \boldsymbol{r}_j) \le n\delta, \mathcal{R}(\boldsymbol{r}_i) = \mathcal{R}(\boldsymbol{r}_j)\big\},$$

where $n \in \{0, 1, 2, ...\}$ is index of the set, and δ is discretization spacing distance, e.g., $\delta = 1$ m, and $\mathcal{R}$ is the region of location $\boldsymbol{r}_i$ (from Fig. 4). We imposed the condition $\mathcal{R}(\boldsymbol{r}_i) = \mathcal{R}(\boldsymbol{r}_j)$ to provide smoothness on correlation values, as the transition from one point to the other is restricted in the actual environment, e.g., see Fig. 1. Nevertheless, we observed that dropping this condition has a low impact on the results. Then for $\Delta \approx n\delta$, we calculate the correlation according to

$$C_{b,b'}(\Delta) \approx \tilde{C}_{b,b'}(n\delta) = \frac{1}{|\mathcal{G}_n|} \times \frac{\sum_{\boldsymbol{r}_i, \boldsymbol{r}_j \in \mathcal{G}_n} (S_b(\boldsymbol{r}_i) - \bar{\mu}_{n,b})(S_{b'}(\boldsymbol{r}_j) - \bar{\mu}_{n,b'})}{\bar{\sigma}_{n,b}\bar{\sigma}_{n,b'}}, \quad (6)$$

where $\bar{\mu}_{n,b} = \frac{1}{|\mathcal{G}_n|}\sum_{\boldsymbol{r}_i \in \mathcal{G}_n} S_b(\boldsymbol{r}_i)$, $\bar{\sigma}_{n,b} = \frac{1}{|\mathcal{G}_n|}\sum_{\boldsymbol{r}_i \in \mathcal{G}_n}(S_b(\boldsymbol{r}_i) - \bar{\mu}_{n,b})^2$, similar relations hold for $\bar{\mu}_{n,b'}$ and $\bar{\sigma}_{n,b'}$ but using $\boldsymbol{r}_j$ and b'. Note that we use (6) also to calculate single-band correlations, $b = b' = c$ or $b = b' = m$.

To assess the performance of the proposed models we consider the two single-band correlation examples, eqs. (1) and (2). Figures 6 and 7 show the empirical and fitted models for both cases, respectively. The relevant parameters are provided, respectively, in Tab. IV and Tab. V. We evaluate

the goodness of fit using Adjusted R-Squared and Error Sum of Squares (SSE) metrics.

A. The proposed models

For the Gudmundson model (1), we notice from Tab. IV that both proposed models provide similar performance, with approximately similar frequency correlation coefficient and decorrelation distances, this is also observed in Fig. 6. For the modified Gudmundson model (2), both of our models still provide comparable results, however, as Fig. 7 and the goodness of fit in Tab. V suggest, model 1 seems to slightly outperform the second model.

When fitting the empirical correlation to the models, we initially used the general forms, i.e., (α_c, α_m), and (β_c,β_m). However, the resultant values were not stable and were estimated within large confidence intervals. We also did not observe much improvement in the goodness of fit, thus we focused on the presented special cases. For both models, in both cases, setting $\alpha_c = 0.5$ and $\beta = 0.5$ did not result in a significant change in the SSE values, but have improved the adjusted R-squared. Thus, the choice of $\alpha_c = 0.5$ and $\beta = 0.5$ for this environment indicates that both arithmetic and geometric means are valid cross-band correlation techniques, making them reasonable choice when only ρ and the spatial correlations in both bands are available.

From Figs. 6 and 7, we observe that the empirical cross-band correlation function is different from $\rho C_{b,b}$ (a scaled version of a single-band spatial correlation function). We notice that, in this environment, $\rho C_{c,c}$ overestimates the correlation, while $\rho C_{m,m}$ underestimates it. To quantify that, we calculated the SSE for the cross-band correlation function $C_{b,b'}$ when fitted to model 1 and model 2, and for $\rho C_{b,b}$, the results are shown in Tables IV and V. We notice that the SSE values for $\rho C_{b,b}$ are approximately twice those of the proposed models.

B. The environment

The tables also provide insights about the environment. From Tab. IV, we notice that decorrelation distances for both bands are relatively short. Similar values were also observed in a number of other environments, such as indoor and industrial environments [17], where the decorrelation distance could be in the range of 5 m and may fall below 0.5 m. We also notice that the decorrelation distance is shorter in the mmWave band, this is reasonable as objects throw "sharper shadows" at higher frequencies.

From the figure and the tables, we also observe that the modified Gudmundson model provides a better fit to the shadowing correlation, where the parameters γ_b allow us to match the curvature at small distances.

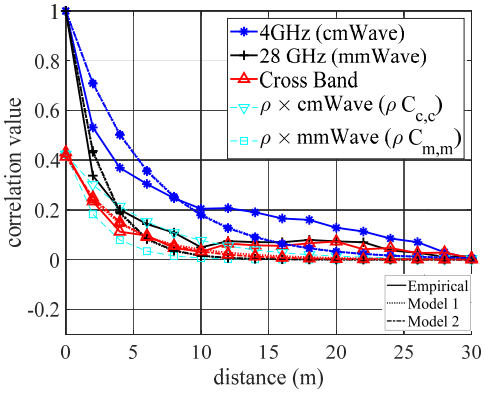

Fig. 6: Correlation values over distance for the two proposed models for the Gudmundson model (1).

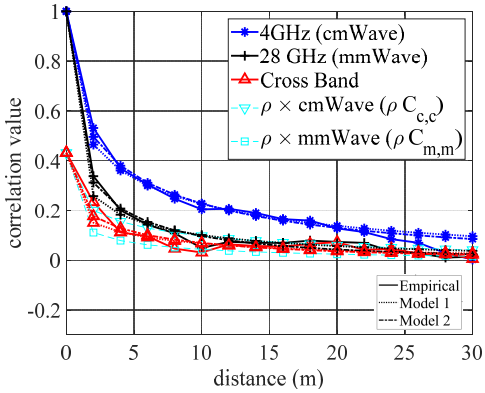

Fig. 7: Correlation values over distance for the two proposed models for the modified Gudmundson model (2).

TABLE IV: Cross band correlation parameters with underlying Gudmundson single band model.

Parameters	**Model 1**	**Model 2**
α_c	.48	N/A
β	N/A	.43
$(d_{\text{cor},c}, d_{\text{cor},m})$	(4.06,1.165)	(4.01,1.67)
ρ	.42	.41
Adjusted R-Squared	0.89	0.89
SSE	0.17	0.18
SSE ($C_{c,m}$ only)	0.025	0.031
	$\rho\mathbf{C_{c,c}}$	$\rho\mathbf{C_{m,m}}$
SSE ($C_{c,m}$ only)	0.048	0.05

TABLE V: Cross band correlation parameters with underlying modified Gudmundson single band model (eq. (2))

Parameters	**Model 1**	**Model 2**
α_c	.44	N/A
β	N/A	0.48
$(d_{\text{cor},c}, d_{\text{cor},m})$	(2.64,0.55)	(2.97,0.97)
(γ_c, γ_m)	(0.41,.33)	(0.46,.43)
ρ	.43	.43
Adjusted R-Squared	0.991	0.987
SSE	0.013	0.019
SSE ($C_{c,m}$ only)	0.01	0.013
	$\rho\mathbf{C_{c,c}}$	$\rho\mathbf{C_{m,m}}$
SSE ($C_{c,m}$ only)	0.026	0.02

VI. Conclusions

In this paper, we proposed cross-band shadowing correlation models, which capture the correlation in space and frequency for wireless systems that operate in cmWave and mmWave bands. We designed the models such that it is possible to integrate existing single frequency band correlation models. We applied the proposed model, considering two single-band spatial correlation examples, to channels in a micro-cellular environment. The results signify the importance of using cross-band correlation functions to capture the joint correlation properties in the two bands. In particular, we observed that using scaled single-band spatial correlation to represent the cross-band correlation doubles the SSE. Interestingly, the results, for the studied environment, suggest that using average of the spatial correlation might be a good approximation to capture the cross-band correlation.

There are several relevant research directions that can be considered for future work. The feasibility of the proposed model is important, as it impacts the practicality of the models. Parameterization for a larger number of environments, based on extensive deterministic predictions or measurements, is necessary. Finally, the generalization to cover multiple (beyond two) frequency bands is also interesting.

VII. Acknowledgement

This work was financially supported by a National Science Foundation WiFiUS grant 1457340 and by the Academy of Finland WiFiUS grant 284709.

References

[1] A. F. Molisch, *Wireless Communications*. Wiley; 2 edition, 2010.

[2] N. Patwari and P. Agrawal, "Effects of correlated shadowing: Connectivity, localization, and RF tomography," in *2008 International Conference on Information Processing in Sensor Networks (IPSN 2008)*. IEEE, 2008, pp. 82–93.

[3] A. Conti, M. Z. Win, M. Chiani, and J. H. Winters, "Bit error outage for diversity reception in shadowing environment," *IEEE Communications Letters*, vol. 7, no. 1, pp. 15–17, 2003.

[4] M. Gudmundson, "Correlation model for shadow fading in mobile radio systems," *Electronics letters*, vol. 27, no. 23, pp. 2145–2146, 1991.

[5] K. Chandra, R. V. Prasad, B. Quang, and I. Niemegeers, "CogCell: cognitive interplay between 60 GHz picocells and 2.4/5 GHz hotspots in the 5G era," *IEEE Communications Magazine*, vol. 53, no. 7, pp. 118–125, 2015.

[6] D. Burghal and A. F. Molisch, "Rate and outage probability in dual band systems with prediction-based band switching," *IEEE Wireless Communications Letters*, vol. 7, no. 5, pp. 872–875, 2018.

[7] V. Kristem, C. U. Bas, R. Wang, and A. F. Molisch, "Outdoor wideband channel measurements and modeling in the 3–18 GHz band," *IEEE Transactions on Wireless Communications*, vol. 17, no. 7, pp. 4620–4633, 2018.

[8] S. S. Szyszkowicz, H. Yanikomeroglu, and J. S. Thompson, "On the feasibility of wireless shadowing correlation models," *IEEE Transactions on Vehicular Technology*, vol. 59, no. 9, pp. 4222–4236, 2010.

[9] D. Catrein and R. Mathar, "Gaussian random fields as a model for spatially correlated log-normal fading," in *2008 Australasian Telecommunication Networks and Applications Conference*. IEEE, 2008, pp. 153–157.

[10] Y. Zhang, J. Zhang, D. Dong, X. Nie, G. Liu, and P. Zhang, "A novel spatial autocorrelation model of shadow fading in urban macro environments," in *IEEE GLOBECOM 2008-2008 IEEE Global Telecommunications Conference*. IEEE, 2008, pp. 1–5.

[11] P. Agrawal and N. Patwari, "Correlated link shadow fading in multi-hop wireless networks," *IEEE Transactions on Wireless Communications*, vol. 8, no. 8, pp. 4024–4036, 2009.

[12] Z. Wang, E. K. Tameh, and A. R. Nix, "Joint shadowing process in urban peer-to-peer radio channels," *IEEE Transactions on Vehicular Technology*, vol. 57, no. 1, pp. 52–64, 2008.

[13] A. Sibille, "Efficient generation of spatially and frequency correlated random values for cognitive radio network simulators," *IEEE Transactions on Vehicular technology*, vol. 59, no. 3, pp. 1121–1128, 2010.

[14] K. Sato, K. Inage, and T. Fujii, "Frequency correlation of shadowing over TV bands in suburban area," *Electronics Letters*, vol. 54, no. 1, pp. 6–8, 2017.

[15] B. Van Laethem, F. Quitin, F. Bellens, C. Oestges, and P. De Doncker, "Correlation for multi-frequency propagation in urban environments," *Progress In Electromagnetics Research*, vol. 29, pp. 151–156, 2012.

[16] B. Zhang, Z. Zhong, K. Guan, R. He, and C. Briso-Rodríguez, "Shadow fading cross-correlation of multi-frequencies in curved subway tunnels," in *17th International IEEE Conference on Intelligent Transportation Systems (ITSC)*. IEEE, 2014, pp. 1111–1116.

[17] E. Tanghe, W. Joseph, L. Verloock, L. Martens, H. Capoen, K. Van Herwegen, and W. Vantomme, "The industrial indoor channel: large-scale and temporal fading at 900, 2400, and 5200 MHz," *IEEE Transactions on Wireless Communications*, vol. 7, no. 7, pp. 2740–2751, 2008.

[18] P. Koivumäki, S. L. Nguyen, K. Haneda, and G. Steinböck, "A study of polarimetric diffuse scattering at 28 GHz for a shopping center facade," in *2018 IEEE 29th Annual International Symposium on Personal, Indoor and Mobile Radio Communications (PIMRC)*. IEEE, 2018, pp. 182–187.

[19] J. Monserrat, R. Fraile, and L. Rubio, "Application of alternating projection method to ensure feasibility of shadowing cross-correlation models," *Electronics Letters*, vol. 43, no. 13, pp. 724–725, 2007.

[20] M. Peter *et al.*, "Measurement campaigns and initial channel models for preferred suitable frequency ranges," Deliverable D2.1, Mar. 2016.

[21] ——, "Measurement results and final mmMAGIC channel models," Deliverable D2.2, May 2017.

[22] A. Torabi, S. A. Zekavat, and K. Sarabandi, "Wideband directional channel characterization for multiuser MIMO systems over a random rough dielectric ground," *IEEE Transactions on Wireless Communications*, vol. 15, no. 5, pp. 3103–3113, May 2016.

[23] C. Jansen, S. Priebe, C. Moller, M. Jacob, H. Dierke, M. Koch, and T. Kurner, "Diffuse scattering from rough surfaces in THz communication channels," *IEEE Transactions on Terahertz Science and Technology*, vol. 1, no. 2, pp. 462–472, Nov. 2011.

[24] O. Landron, M. J. Feuerstein, and T. S. Rappaport, "A comparison of theoretical and empirical reflection coefficients for typical exterior wall surfaces in a mobile radio environment," *IEEE Transactions on Antennas and Propagation*, vol. 44, no. 3, pp. 341–351, Mar. 1996.

[25] U. T. Virk, S. L. H. Nguyen, K. Haneda, and J. Wagen, "On-site permittivity estimation at 60 GHz through reflecting surface identification in the point cloud," *IEEE Transactions on Antennas and Propagation*, vol. 66, no. 7, pp. 3599–3609, Jul. 2018.

[26] ITU-R P.2040, "Effect of building material and structures on radio wave propagation above about 100 MHz," Jul. 2015.

[27] J. Järveläinen, S. L. H. Nguyen, K. Haneda, R. Naderpour, and U. T. Virk, "Evaluation of millimeter-wave line-of-sight probability with point cloud data," *IEEE Wireless Communications Letters*, vol. 5, no. 3, pp. 228–231, Jun. 2016.

[28] J. Järveläinen, K. Haneda, and A. Karttunen, "Indoor propagation channel simulations at 60 GHz using point cloud data," *IEEE Transactions on Antennas and Propagation*, vol. 64, no. 10, pp. 4457–4467, Oct. 2016.